Craze behaviour in isotactic polystyrene: 1. Craze–spherulite interaction

Donald E. Morel and David T. Grubb
Department of Materials Science and Engineering and the Materials Science Center, Cornell University, Ithaca, NY 14853-0121, USA
(Received 4 March 1983)

The deformation of isotactic polystyrene (i-PS) in uniaxial tension at room temperature has been studied in detail by transmission electron microscopy. Quantitative analysis reveals that crazes in amorphous i-PS are similar to crazes formed in atactic polystyrene (a-PS) under the same conditions, except for a higher stress concentration at the craze tip. Fully spherulitic i-PS films contain crazes with very irregular paths which often nucleate at spherulite triple points. Craze–spherulite interactions have been observed in films which contain spherulites isolated in an amorphous matrix. Lamellae with their c-axis perpendicular to the tensile axis generally yield a higher craze fibril draw ratio than in the amorphous matrix. Lamellae with their c-axis parallel to the tensile axis cause a decrease in both λ and craze width. When the c-axis is in the plane of the film but oblique to the tensile axis, the craze deviates toward the centre of the spherulite. The entanglement network approach applied to crystalline i-PS predicts the correct anisotropic behaviour of λ when neutron scattering data on chain conformation in i-PS crystals are used.

Keywords Crazing; isotactic-polystyrene; spherulite; orientation; entanglement; crystalline

INTRODUCTION

Crazing

Tensile deformation of glassy polymers to high draw ratios can occur by a number of mechanisms, including homogeneous deformation, crazing, or the formation of plastic deformation zones. Crazes are crack-like defects which grow normal to the direction of the applied tensile stress. However, they are not true cracks; rather, they consist of two sharp interfaces which are spanned by fine polymer fibrils.[1-3] These fibrils maintain the mechanical integrity of the material and, therefore, the craze is capable of sustaining some load. Crazes formed in atactic polystyrene typically consist of 75% voids and 25% fibrillated material, with fibril diameter of the order of 6 nm[4-6]. In air, crazes thicken primarily by drawing in new material at the craze–bulk interface, i.e. by the surface drawing mechanism[7]. Crazing in plasticizing environments, such as organic solvents, leads to increased molecular mobility in the fibrils and craze thickening by fibril creep[3].

Crazes are fundamental in determining the fracture behaviour in both isotropic and oriented glassy polymers. They are simultaneously a primary source of fracture toughness and precursors to crack formation and eventual failure. The relatively high fracture toughness of many glassy polymers is directly attributable to dissipation of energy as a result of craze formation. Crazes can then act as preferred paths for crack propagation due to fibril breakdown. As a result of their fundamental role in fracture properties, much work has been carried out recently on the micromechanics and microstructure of crazes in amorphous glassy polymers[3-14].

Spherulite deformation

Spherulites are the normal result of the quiescent crystallization of polymers from the melt. These structures consist of a radiating array of crystalline lamellae separated by layers of amorphous and non-crystallizable material. In i-PS, the average crystallinity of a spherulite is approximately 50%[15,16].

Deformation processes occurring in spherulites are not well understood, due to the complex initial morphology of the spherulite and the high degree of mechanical anisotropy of the component crystals. A large number of competing processes have been observed to contribute to low draw ratios. These include crystallographic mechanisms such as twinning and phase transformation, chain and lamellar slip, and deformation of the amorphous regions sandwiched between crystalline lamellae[17]. At large draw ratios, the spherulitic structure is completely destroyed and transforms into a microfibrillar structure. Each microfibril consists of small crystallites the chain direction of which is oriented parallel to the tensile direction, which are connected by partially extended chains constituting the interlamellar non-crystalline regions[18-20].

A number of studies on the microstructural changes in spherulite deformation have been carried out using light microscopy, light scattering, and electron microscopy[21-32]. These experiments have used thin films or sections microtomed from material deformed in the bulk. The materials investigated have been mainly polyethylene, isotactic polypropylene, polyoxymethylene, and polybutene-1. All studies were carried out on fully spherulitic films so that the stress field in the film was highly irregular. The resulting deformation behaviour

0032-3861/84/030417-13$03.00

depends strongly on the thermal history of the material in question. Limited deformation would be either inter- or intra-spherulitic, and failure could occur in either a brittle or ductile mode.

This study describes craze behaviour in a semi-crystalline polymer deformed below the T_g of the amorphous material. Working below T_g allows spherulites isolated in an amorphous matrix to be obtained. Local interactions between the craze and spherulite lamellae are then readily observed in the TEM. Observations of the deformation behaviour of the craze as it crosses the amorphous–crystalline boundary illustrate the effects of crystallinity on deformation. In addition, these results can be compared with the effects of varying entanglement network density[33] and pre-orientation[34] on craze properties.

EXPERIMENTAL

Sample preparation

The isotactic polystyrene ($\bar{M}_n = 87\,000$, $\bar{M}_w = 518\,000$) used in this investigation was kindly supplied by Dr R. Bubeck of Dow Chemical Company. Prior to use, the granules were extracted for 24 h in methyl ethyl ketone at 90°C to remove any atactic material present. The remaining i-PS was then dried at 100°C for 24 h *in vacuo* to remove any residual solvent.

Thin films were prepared from solutions of i-PS in hot dichlorobenzene. The films were cast onto microscope slides by pulling the slides slowly from the solution. Film thickness is controlled by the concentration of i-PS in the solvent; 1% (by weight) solutions were used for the determination of crystal growth rate, yielding film thicknesses of 100 nm. For craze and TEM specimens, 400 nm films were produced from a 2.5% i-PS solution.

To measure crystal growth rates, films were maintained at 250°C for 10 min, quenched to the desired crystallization temperature, and isothermally crystallized for 1–6 h at temperatures ranging from 120° to 200°C using a Mettler FP5 hot stage accurate to within ±0.2°C. Spherulite diameters were measured with a Leitz polarizing microscope fitted with a micrometer eyepiece. Measurement of the spherulitic growth rate served two purposes: (1) it established the quality of the i-PS, and (2) it provided data on annealing time and temperature to produce spherulites of a certain size in an amorphous matrix.

Resulting spherulite growth data are shown in *Figures 1* and *2*, and agree well with previously published data for i-PS[35–37]. *Figure 1* shows a rectilinear increase in spherulite size with increased annealing time at a given crystallization temperature, T_c. *Figure 2* shows log G (growth rate) *versus* T_c. G increases reasonably rapidly to G_{max} at approximately 175°C, and then declines in an approximately symmetrical fashion. This data was used to predict t_c (crystallization time), and T_c (crystallization temperature) to produce spherulites of a desired size. Specimens for examination in the TEM were produced by bonding 400 nm thick films to annealed copper grids. This was accomplished by floating the film off the glass slide onto the surface of a distilled water bath. The copper grid, pre-coated with a 3% a-PS solution, is then used to pick up the film. Final bonding is achieved by exposure of the film to toluene vapour for 15–30 s. This method was

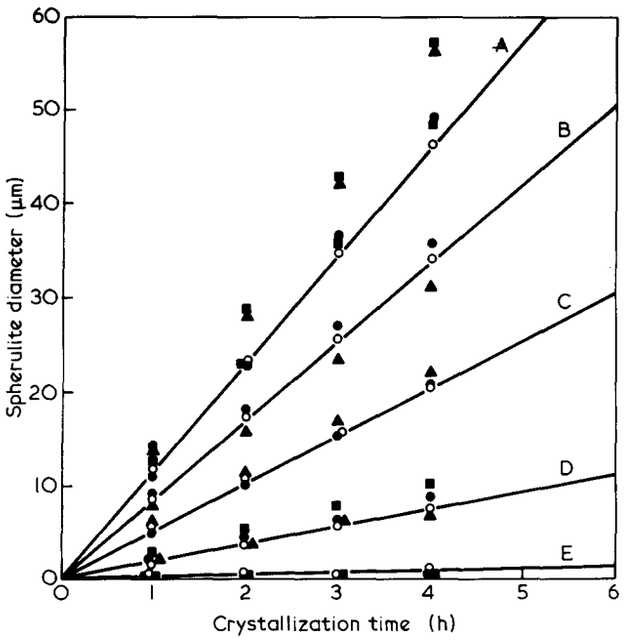

Figure 1 Spherulite diameter as a function of crystallization time. A, 180; B, 160; C, 200; D, 140; E, 120°C. ●, From ref. 35; ■, from ref. 36; ▲, from ref. 37; ○, current study

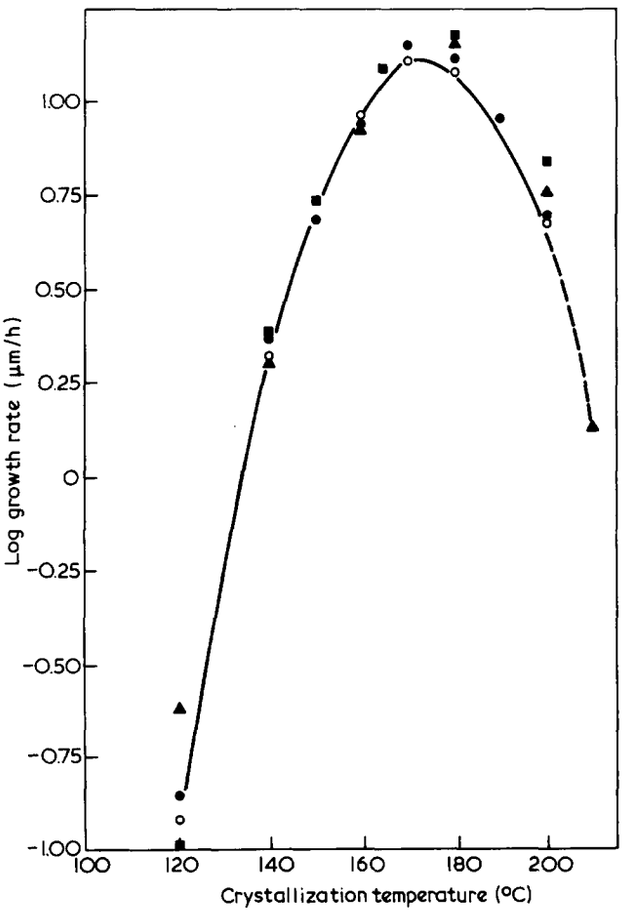

Figure 2 Spherulite growth rate as a function of crystallization temperature. ●, From ref. 35; ■, from ref. 36; ▲, from ref. 37; ○, current study

developed by Lauterwasser and Kramer, and is described in full in ref. 4.

Amorphous i-PS films were strained to a nominal strain of 0.7% in air which was maintained for 2 h to allow the crazes to attain equilibrium. Craze formation was observed optically; grid squares seen to contain suitable crazes were cut out for examination in the TEM. Relaxation of the crazes is prevented by the irreversible plastic deformation of the copper grid. Semi-crystalline specimens were produced by annealing grid mounted amorphous i-PS samples in the Mettler hot stage. Annealing times were chosen to yield the desired spherulite sizes using the crystal growth rates obtained as described previously. Following crystallization, grids were strained at 0.7% for 2 h and prepared for TEM exactly as for the amorphous samples.

Annealing at $T_c > 175°C$ resulted in breakdown of the film attached to the copper grid. When crystallized directly on the glass slides, the films could not be removed. Using rock salt as a substrate and removing the salt in a water bath resulted in row structures nucleating along fracture striations on the substrate surface.

Electron microscopy

It is well known that exposure of crystalline polymers to the electron beam results in radiation-induced changes in structure[38-40]. Specimens become disordered, lose mass, and may change their shape and appearance. Generally, long-range order is rapidly destroyed so that the diffraction pattern and diffraction contrast in the image decay. This initial change in structure is followed by a second period of instability in which mass loss and other changes continue. The final result is a stable radiation-damaged structure. Much useful information can be obtained from the final stable configuration as its structure is closely related to, though not identical with, the original one. A radiation-induced enhancement of contrast often occurs in spherulites, resulting in increased visibility of the overall lamellar structure in the damaged specimen[39-40].

Polystyrene is comparatively radiation resistant; its diffraction pattern lasts several times longer than that of polyethylene, and the mass loss and change of chemical composition of a-PS and i-PS are very small even at very high doses. As a result, radiation-induced changes occur more slowly and are less marked. There is little observable change in films of a-PS; this stability is the basis for the quantitative electron microscopy of craze structure in atactic polystyrene. Amorphous i-PS is similarly stable, but crystalline i-PS does visibly change in the electron microscope; these changes are qualitatively similar to those in polyethylene. Crystalline regions of i-PS cease to diffract, become slightly distorted, and become more clearly distinguished from the amorphous matrix[41].

The micrographs of i-PS in this paper have been taken at relatively high radiation doses. Crystalline diffraction has completely decayed, and the changing structural appearance of the spherulites has stabilized. Close attention to these changes indicates the primary result to be an increase in contrast between individual lamellae. All micrographs were taken in a JEOL 200CX microscope at 200 kV. The details of spherulite structure may be less clear than in previously published work because the film thickness used was 400 nm. This is much thicker than films normally used for structural studies; however, this thickness is necessary to ensure that resulting craze structures and mechanical properties are similar to those in bulk polystyrene[5,7].

RESULTS AND DISCUSSION

Micromechanics of crazes in amorphous i-PS

Following the technique developed by Lauterwasser and Kramer[4], a series of electron micrographs were taken along the craze being investigated. The thickness of the craze, T, can be measured directly from the micrographs. The volume fraction of fibrils in the craze, V_f, can be determined locally at points along the craze from microdensitometer measurements of the optical densities, ϕ, of the craze, a hole, and the film. The volume fraction is then given by:

$$V_f = 1 - \frac{\ln[\phi_{craze}/\phi_{film}]}{\ln[\phi_{hole}/\phi_{film}]} \quad (1)$$

This relation is valid providing the exposure is directly proportional to the optical density.

Knowing both T and V_f at specific points along the craze allows computation of all important craze parameters. The draw ratio of the fibrils is:

$$\lambda = T/T_0 = 1/V_f \quad (2)$$

where T_0 is the primordial craze thickness (the original thickness of material prior to being drawn into the craze). The strain in the fibrils can be calculated from:

$$\varepsilon = \ln(\lambda) \quad (3)$$

The craze surface displacement profile, $w(x)$, is then given by:

$$w(x) = \frac{T(x)}{2}[1 - V_f(x)] \quad (4)$$

Knowing $w(x)$ allows computation of $T_0(x)$ as:

$$T(x) = T_0(x) + 2w(x) \quad (5)$$

The craze parameters T, T_0, and w are illustrated schematically in *Figure 3*.

To obtain the total stress acting on the craze surfaces, σ_∞ and $\Delta S(x)$ must be calculated. σ_∞ is the applied stress which acts perpendicular to the direction of craze growth. $\Delta S(s)$ is the set of stresses which would act on the craze to maintain a set of displacements, $w(x)$, in the absence of any applied stress. The total stress acting on the craze is then given by:

$$S(x) = \Delta S(x) + \sigma_\infty \quad (6)$$

σ_∞ can be calculated by multiplying the applied strain by the tensile modulus of the material (≈ 3000 MPa for a-PS and amorphous i-PS). Obtaining the $\Delta S(x)$ profile is slightly more complicated.

To calculate $\Delta S(x)$, Lauterwasser and Kramer developed a Fourier Transform method using the work of Sneddon[42]. Assuming the polymer film to be an infinite, perfectly linear elastic sheet, the craze is modelled as a slit of zero thickness which grows in response to an applied tensile stress at infinity, σ_∞. The craze displacement profile, $w(x)$, is calculated from the values of V_f and T

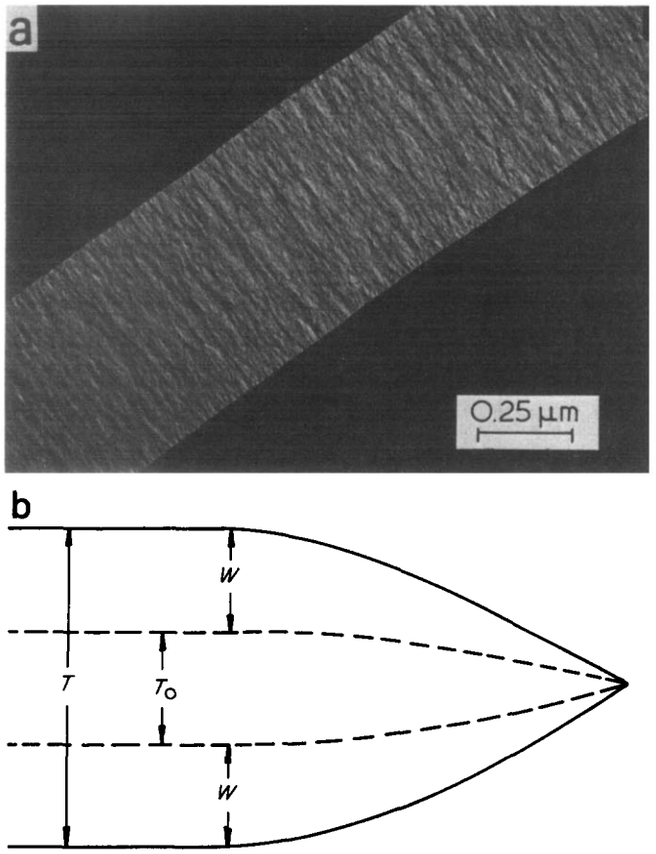

Figure 3 (a) Transmission electron micrograph of an air craze in amorphous i-PS, showing the oriented fibril structure and the sharp craze–matrix interface. (b) Schematic diagram of a craze showing relation between T, T_0, and w^4

measured at various points along the length of the craze from the electron micrographs using equation (4). Once $w(x)$ is known, $\Delta S(x)$ can be obtained by numerical solution of the following equation[4]:

$$\Delta S(x) = -\frac{2}{\pi}\int_0^\infty \tilde{p}(\xi)\cos(x\xi)\mathrm{d}\xi \qquad (7)$$

where

$$\tilde{p}(\xi) = \frac{\xi E}{2}\int_0^a w(x)\cos(x\xi)\mathrm{d}x \qquad (8)$$

a = craze length/2
$w(x)$ = craze opening displacement
E = tensile modulus for plane stress.

This analysis is now applied to an isolated air craze in amorphous i-PS. The results for the craze thickness, fibril extension ratio, and craze opening displacement profiles are shown in *Figures 4–6*; craze surface stress and craze fibril stress are plotted in *Figures 7* and *8*. Lauterwasser and Kramer's results for a similar craze in a-PS are superimposed on those of i-PS for comparison. The crazes analysed here are almost equal in length, but not exactly, with the i-PS craze being slightly larger. In *Figures 4* and *6*, the curves are drawn with the craze centres superimposed. *Figures 5* and *7* are compared with the craze tips superimposed.

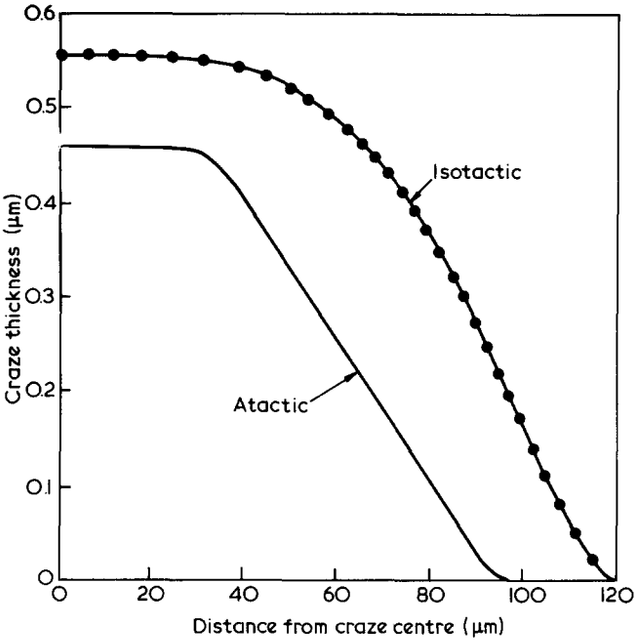

Figure 4 Comparison of air craze geometry and micromechanics in atactic[4] (———) and amorphous isotactic (●—●) polystyrene. Craze thickness profiles, $T(x)$. The greater length and central thickness of the isotactic craze is not significant. The shapes of the crazes are generally similar, but differ in detail

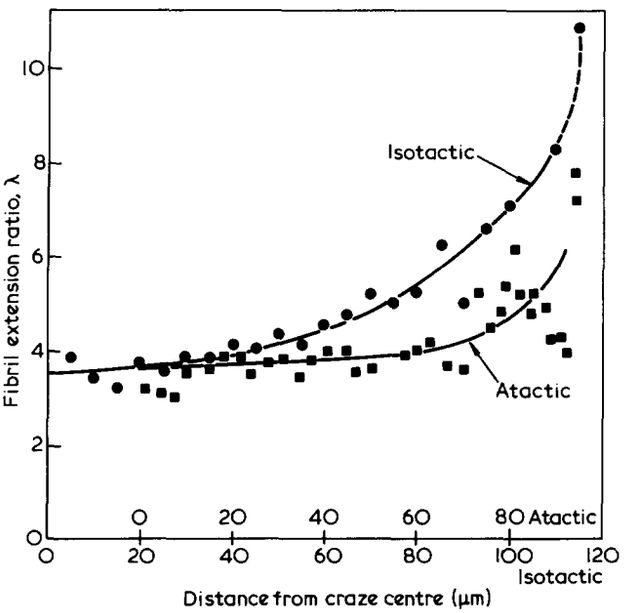

Figure 5 Comparison of air craze geometry and micromechanics in atactic[4] (■) and amorphous isotactic (●) polystyrene. Fibril extension profiles, $\lambda(x)$. As λ is approximately constant near the craze base, and increases sharply near the tip, the a-PS curve is shifted to the right to superimpose the tip on the i-PS tip. This clearly shows the higher extension of the isotactic material

Generally, the craze geometry and micromechanics are very similar. Both crazes reduce in thickness very gradually over approximately 70 μm to a sharp tip. Surface drawing is the predominant mechanism of thickening as the fibril extension ratio remains reasonably constant along the craze, increasing markedly only at the craze tip. If fibril creep were dominant, a significant increase in λ would be expected from craze tip to craze base. The

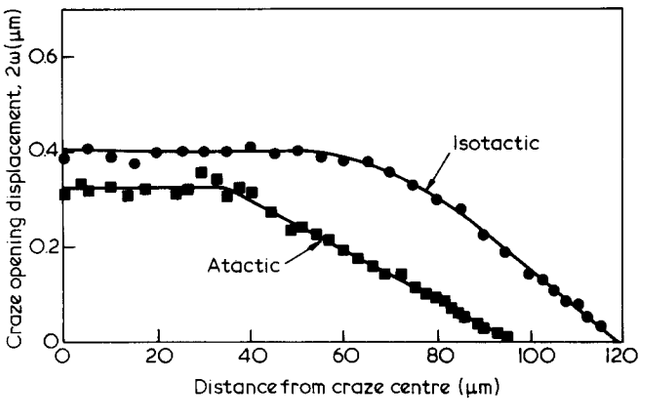

Figure 6 Comparison of air craze geometry and micromechanics in atactic[4] (■) and amorphous isotactic (●) polystyrene. Craze opening displacement profiles, $2w(x)$. As in *Figure 4*, the profiles are generally similar, but differ in detail. (The absolute values are not equal because of the difference in craze size)

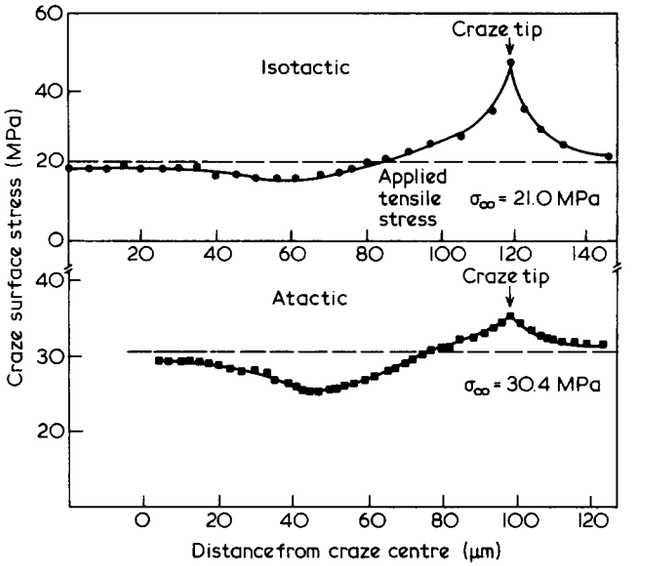

Figure 7 Comparison of air craze geometry and micromechanics in atactic[4] (■) and amorphous isotactic (●) polystyrene. Craze surface stress profiles, $S(x)$. The atactic profile is again shifted to the right to superimpose the tips, as in *Figure 5*. The shapes of the curves for the two materials are similar, the most marked difference being the higher stress concentration at the i-PS tip

surface stress profiles also appear relatively similar. Along the base of the craze, the surface stress is slightly below the applied tensile stress; it then increases to a stress concentration at the craze tip. Finally, in *Figure 8* both materials show a sharp increase in fibril stress, σ_f, with fibril extension ratio.

These overall similarities in mechanical behaviour are expected. Crazes with similar microstructures which have higher fibril extension ratios at their tips than their base, have been seen in a wide range of materials of different properties[33]. It is more instructive to concentrate on the differences between these two amorphous materials which differ only in tacticity. *Figure 4* shows the shapes of the crazes are different; the a-PS thickness profile changes abruptly at 40 μm, after a region of constant thickness at the base, and then decreases gradually to the tip. The i-PS profile is more curved, and becomes steeper as the tip is approached. The fibril extension ratio profiles, *Figure 5*,

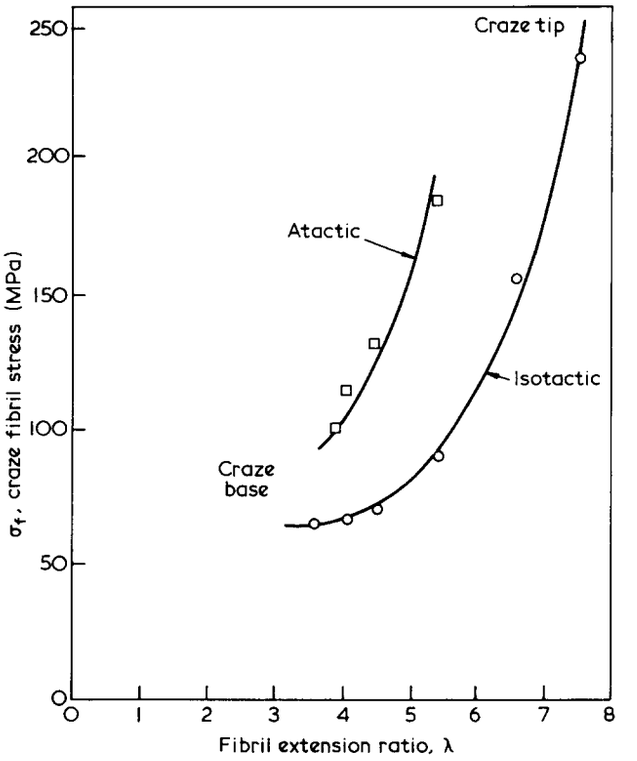

Figure 8 Comparison of air craze geometry and micromechanics in atactic[4] (■) and amorphous isotactic (●). Polystyrene craze fibril stress, σ_f, as a function of extension ratio, λ. The isotactic material is more extended and under higher stress at the tip

are similar near the base, but diverge as the craze tip is approached. The i-PS curve shows the material near the tip to be drawn out more than that near the a-PS tip. A value of $\lambda \approx 11$ was obtained near the i-PS tip, but this value is not very reliable because of the small volume of fibrillated material present and the limiting aperture size of the optical densitometer (dotted line, *Figure 5*). When the T and V_f data ($V_f = 1/\lambda$) are combined to produce the craze opening displacement profile $w(x)$, *Figure 6*, the differences described in *Figure 4* are maintained.

The differences in $w(x)$ can be related to the differences in stress profile, *Figure 7*. The i-PS $w(x)$ profile changes more smoothly from constant displacement near the craze centre resulting in a smoother surface stress profile. The large dip seen in the a-PS craze is not observed. In the i-PS craze, the steeper slope of the $w(x)$ profile near the craze tip results in a significantly higher stress concentration at the tip. The stress concentration factors are $47/21.0 = 2.2$ for i-PS and $35/30.4 = 1.2$ for a-PS. Although the actual peak values of stress rely on an extrapolation of displacement to a sharp tip, the same extrapolation procedure is used in both cases.

The combination of the stress concentration and high extension ratios produce very high fibril stresses ($\sigma_f = \lambda S(x)$) in i-PS near the craze tip; $\sigma_f = 240$ MPa at 7 μm from the tip, approximately 8% of the modulus of the amorphous material, and $\sigma_f = 500$ MPa at the tip itself, using the extrapolated stress concentration. Such large stresses should lead to very rapid fibril failure and breakdown of the craze to form a crack. However, there is diffraction evidence for oriented crystallization in i-PS craze fibrils[43]; such crystals will strengthen the fibrils preventing immediate failure.

The most noticeable difference between the two materials is the greater fibril extension ratios achieved in i-PS. According to the entanglement network theory of crazing[33], this implies a smaller random coil and a greater extended length (or larger molecular weight) between entanglements for the isotactic material. These depend on the conformation of the chains, which is likely to be affected by tacticity. Data are lacking on the mean fully extended chain length of an a-PS chain, and on the entanglement molecular weight for i-PS. Previous calculations used the extended chain length of i-PS[33]. Whatever the molecular reason for the greater fibril extension ratio, the result is that i-PS is a weak and brittle material, in agreement with studies of a range of materials of different λ[33].

Craze behaviour in fully spherulitic films

Fully crystalline films of i-PS were prepared by annealing films 400 nm thick for 17 h at 140°C. The resulting microstructure is shown in *Figure 9*. It is important to note that the structure shown in *Figure 9* has undergone some radiation damage. The 'hairy' appearance of the lamellae becomes more sharply defined as exposure to the electron beam is prolonged[39,49]. The dark lines represent lamellae that are 'edge-on' relative to the electron beam.

'Fully crystalline' i-PS is approximately 50% crystalline; the remainder of the material is thought to be non-crystallizable low molecular weight i-PS and some a-PS which is rejected at the lamellar interfaces during crystallization[15,16]. The non-crystallizable material is not only found between individual lamellae, but also at the radial periphery of the growing spherulites.

Figure 10 shows the nucleation sites of two crazes in a crystalline film strained at 0.5% nominal strain for 2 h. Crazes were found to nucleate preferentially at spherulite boundaries, either at so-called 'triple points' (where three spherulites impinge on one another (*Figure 10A*), or at the interface between a spherulite and a large region of amorphous material (*Figure 10B*). Nucleation was not observed to occur at any spherulite centre. Craze initiation always occurred normal to the direction of the applied tensile stress, which is the minor principle stress trajectory. This behaviour is well documented for a-PS[1,2].

Preliminary examination of the crazes in *Figure 10* indicates a highly irregular and ill-defined craze path. This is more apparent in *Figure 11*, which shows a mature craze in a fully crystalline film strained at 0.7%. Unlike air crazes in amorphous i-PS and a-PS, the craze-bulk interfaces do not remain distinctly parallel. Instead, the craze twists and bends as it interacts with the spherulites.

Points (1) and (2) in *Figure 11* show dark regions in the craze with no apparently distinguishable fibril structure. The craze has deviated so that the craze plane is no longer normal to the film place, thus the craze is tilted relative to the electron beam and does not appear in simple projection. This interpretation is supported by the appearance of tilted air crazes in a-PS which have a similar appearance in the TEM[44].

Points (3) and (4) show the considerable variation in craze width which can occur. At point (3), the craze is 0.03 μm wide, at point (4), it is 0.12 μm. This implies that the craze has more difficulty in thickening in some regions than in others. If so, differences in the volume fraction, V_f, of fibrils present in the craze would be expected at points of different width and, hence, there would be different fibril extension ratios, λ.

It is clear that the orientation of individual spherulites relative to the path of the craze has a profound effect on the structure and propagation of the craze, but the

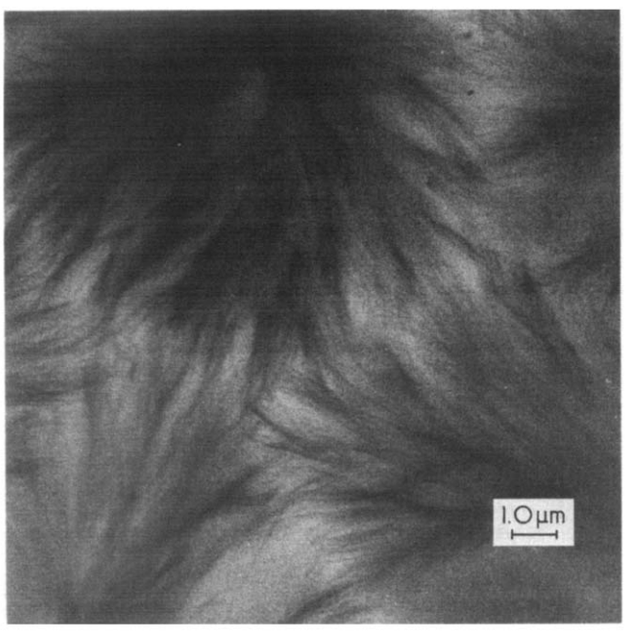

Figure 9 Electron micrograph of a fully spherulitic film after irradiation

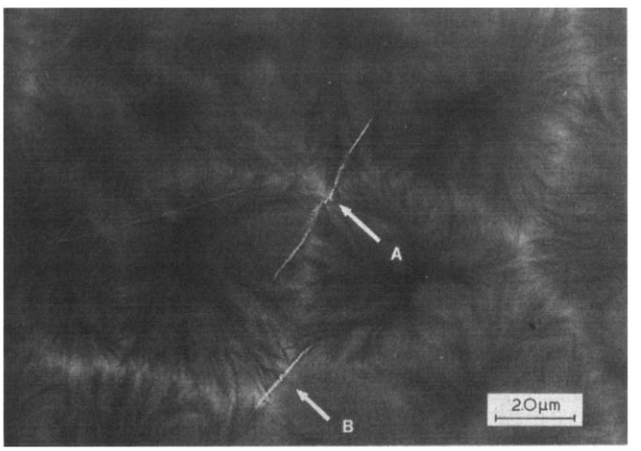

Figure 10 Electron micrograph showing craze nucleation in a fully spherulitic film. At spherulite boundaries crazes grow perpendicular to the applied stress

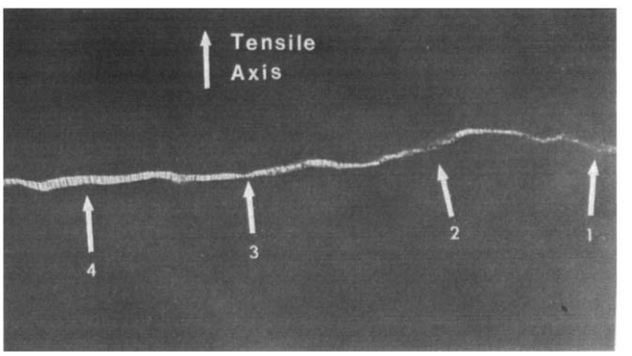

Figure 11 Electron micrograph of a craze in a fully spherulitic film showing highly irregular craze structure

situation in fully crystallized films is too complicated for analysis. These observations are clarified by producing isolated craze–spherulite interactions.

Morphology of isolated craze–spherulite interactions

Films 400 nm thick were annealed at 140°–160°C for 10–20 min prior to straining to produce spherulites isolated in an amorphous matrix. *Figure 12* shows the appearance of a spherulite isolated in an amorphous matrix in the TEM after irradiation. The structure appears very different to that in *Figure 9* because the scale is different. With the same number of nucleating sites for spherulitic growth, isolated spherulites are produced by short crystallization times to yield spherulites 2 μm across, corresponding to the central regions of spherulites in *Figure 9*. The structure in *Figure 12* is clearly that of a sheaf, a term applied to spherulites in an early stage of development[45]. The main bundle of radiating lamellar crystals is darker than the amorphous matrix, and individual lamellae are visible at the outer edge of the spherulite. On either side of the sheaf are light regions with little or no discernible structure.

Although lamellae of all orientations relative to the film plane will occur in the spherulite, those which appear dark (especially those individually visible) can be characterized as being viewed 'edge-on'[40]. The normals to the planes of lamellae of this type lie close to the plane of the specimen film. Neglecting chain obliquity, the lamellar normals are the molecular chain axes of the molecules in the crystal. Transmission electron microscopy of polyethylene and row nucleated i-PS indicates that those crystalline areas appearing lighter after irradiation have their molecular chain axes perpendicular to the film plane[41]. These lamellae lie in the plane of the film, and are termed 'flat-on'. Similar structures have been seen in melt-crystallized thin films of diene polymers[46–48]. In more fully developed spherulites, sections of 'edge-on' and 'flat-on' lamellae are still clearly distinguished. Thus, even when a circular boundary has developed, the spherulite does not have a circularly symmetric structure (*Figures 17–20*). 'Edge-on' and 'flat-on' lamellae are shown schematically in *Figure 13*.

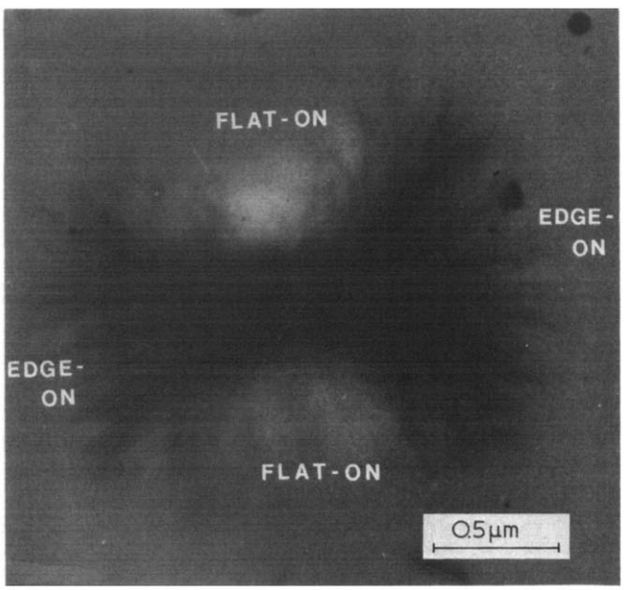

Figure 12 Electron micrograph of an isolated spherulite following irradiation

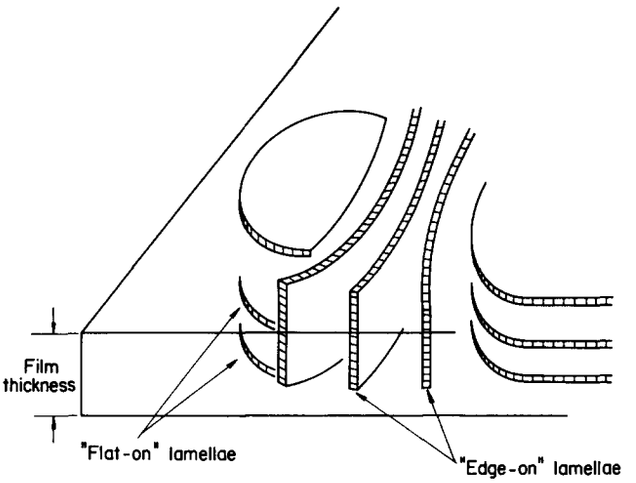

Figure 13 Schematic of a spherulite in a thin film illustrating 'edge-on' and 'flat-on' lamellar configurations

When the film is strained, crazes are formed which can interact with the spherulites in a variety of ways. Because these spherulites do not have full radial symmetry, these interactions can be complicated. However, there are generally four distinct classes into which all interactions can be divided.

Case 1: The craze does not pass through the spherulite, but its path is altered as a result of the inhomogeneous stress field produced in the matrix by the stiffer spherulite.

Case 2: The craze propagates through the periphery of the spherulite with little deviation from its original path.

Case 3: The craze propagates directly through the spherulite centre. Deviations from the initial path of the craze can be large or small depending on the relative orientation of the sheaf axis to the craze path.

Case 4: The craze enters the spherulite but does not pass completely through; i.e. the craze tip is embedded in the spherulite.

These four cases are discussed in detail later; examples are shown in *Figures 14–22*.

Two micrographs are necessary to show each interaction; one micrograph for spherulite structure, and one for the craze structure. This is because the spherulite lamellae are low contrast objects in a thick film, requiring long exposure times for a good image, while the craze is a high contrast object, of much lower mass thickness, therefore requiring a much shorter exposure time. It is difficult to obtain reasonable images of both craze and spherulite on one negative. Even if this can be done, it is impossible to obtain a satisfactory print containing both spherulite and craze structure from such a negative.

In each case, the craze thickness, T, volume fraction, V_f, fibril extension ratio, λ, orientation, and microstructure vary as the craze interacts with the spherulite. Because these parameters can all vary widely in amorphous i-PS (for example, λ ranges from ≈ 4 to ≈ 12 moving from base to tip) comparisons must be made locally with the same craze inside and outside the spherulite. *Table 1* summarizes such comparisons for V_f and, the average draw ratio $\bar{\lambda}$, for the crazes shown in *Figures 14–22*. In some cases, large variations in V_f occur inside the spherulite corresponding to the variable craze structure seen in the micrographs.

Case 1. Here, the craze interacts with the inhomogeneous stress field produced by the rigid crystalline

Table 1 Craze fibril volume fractions (V_f) and draw ratios (λ_m) in the matrix and (λ_s) in the spherulite

	In amorphous matrix		Within spherulite boundaries					
	V_f	$\bar{\lambda}_m$	V_f		$\bar{\lambda}_s$	λ_s/λ_m		
Case 1	0.18–0.23	4.9	0.16–0.21		5.4	1.1		
			Edge-on			Flat-on		
			V_f	$\bar{\lambda}_s$	$\bar{\lambda}_s/\lambda_m$	V_f	$\bar{\lambda}_s$	$\bar{\lambda}_s/\lambda_m$
Case 2 (A)	0.15–0.18	6.1	0.21–2.29	4.0	0.66	–	–	–
(B)	0.20–0.25	4.4	–	–	–	0.19–0.23	4.8	1.1
Case 3 (A)	0.21–0.24	4.4	0.35–0.67	2.0	0.44	–	–	–
(B)	0.18–0.24	4.8	0.26–0.62	2.3	0.48	0.20–0.24	4.5	0.96
(C)	0.22–0.24	4.3	0.20–0.71	2.2	0.51	–	–	–
(D)	0.25–0.27	3.8	–	–	–	0.18–0.22	5.0	1.3
Mean values		4.7 ± 0.6		2.6 ± 0.9	0.5 ± 0.1		4.8 ± 0.2	1.1 ± 0.2
Corrected mean values				3.1 ± 0.9	0.6 ± 0.1		4.4 ± 0.2	1.0 ± 0.2

spherulite in the softer amorphous matrix. The craze does not directly intersect the crystalline lamellae, but it is deviated slightly from its initial path. An interaction of this type is shown in *Figure 14*. The perturbation in the stress field produced by a circular inclusion is shown schematically in *Figure 15* where the modulus of the inclusion (spherulite), E_1, is greater than that of the matrix, E_2.

The thickness of the craze remains constant in the amorphous matrix, but decreases slightly within 1.0 μm from where the craze brushes the spherulite edge (described as 'within spherulite boundaries' in *Table 1* for comparison). The fibril volume fraction, V_f, in the amorphous matrix ranges from 0.18 to 0.23, which corresponds to an average draw ratio $\bar{\lambda}$, of 4.9. These values are within the typical range for air crazes in amorphous i-PS and a-PS.

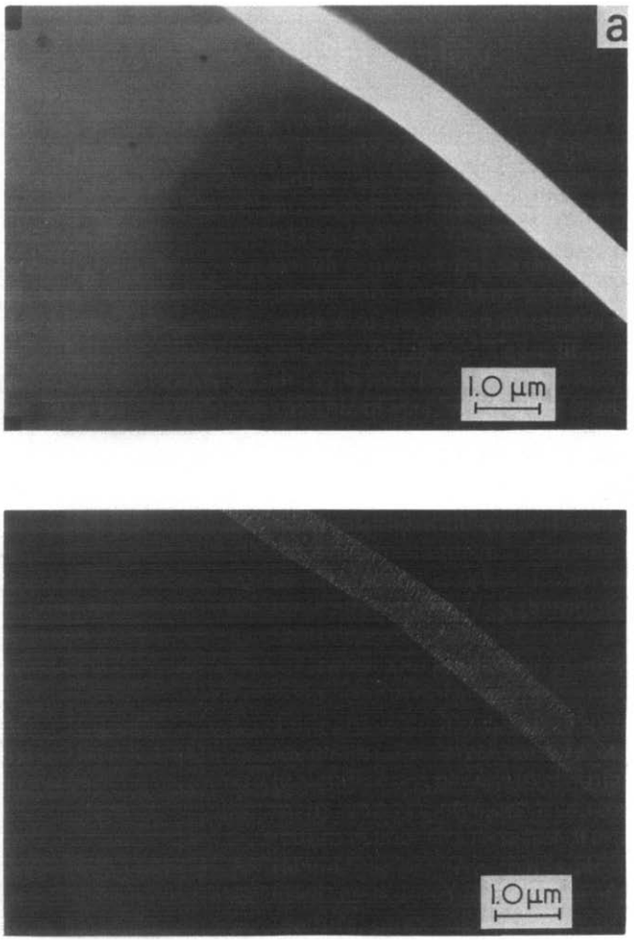

Figure 14 Electron micrographs showing Type 1 interaction where the craze deviates without touching the spherulite

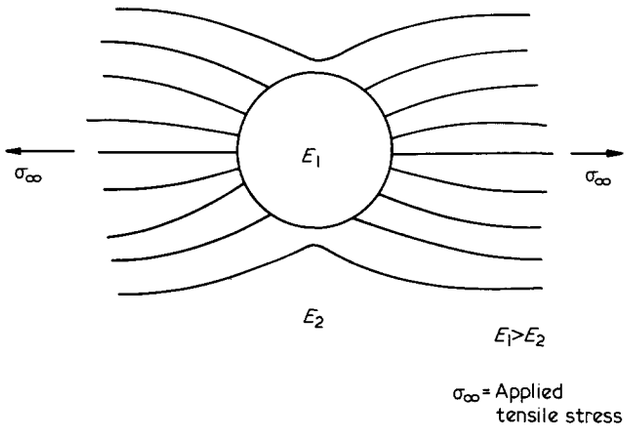

Figure 15 Schematic diagram of stress field associated with a circular inclusion (Modulus E_1) in a matrix (Modulus E_2) where $E_1 > E_2$

In the region where the craze brushes the outer edge of the spherulite, a slight decrease in V_f is observed to 0.16–0.21. This yields an increased draw ratio, $\bar{\lambda} = 5.4$. *Figure 15* indicates this region is one of increased stress, as the spherulite is a stiff inclusion. From the previous micromechanical analysis, it is known that the increased stress associated with the craze tip produces a higher draw ratio. Because the spherulite is a composite of poorly defined anisotropic elements, it is not possible to calculate a stress concentration factor for it, but its magnitude can be estimated using the craze analysed in *Figures 4–8* as a model. From *Figure 5*, the positions where the draw ratio is 4.9 and 5.4 are just above and below 80 μm from the craze centre. The stresses at these positions, from *Figure 7*, are in the ratio 1:1.15. Thus, close to the spherulite the surface stress is some 15% greater.

The craze thickness, T, decreases where $\bar{\lambda}$ increases, and as $\lambda = 1/V_f = T/T_0$, a decrease in primordial craze thickness, T_0 (original thickness of the deformed material), must occur. In this particular example, the variation of T

and V_f results in an almost constant surface displacement, $w(x)$. Thus, the reduced craze thickness may be due to the spherulitic material resisting drawing, or to external constraints which may require a constant local opening displacement $w(x)$.

Case 2. Two different interactions are possible in Case 2; these are illustrated in *Figures 16a* and *b*. For Type 2a interactions the craze intersects mainly edge-on lamellae. In Type 2b interactions, the craze intersects mainly flat-on lamellae. In both cases, craze thickness and V_f remain constant in the matrix; differences in these parameters arise when the craze propagates through the spherulite.

When the craze interacts with edge-on lamellae, the craze thickness decreases (from 0.1 μm to 0.07 μm in *Figure 16a*). V_f increases where the craze intersects the lamellae from 0.15–0.18 in the matrix to 0.21–0.29 in *Figure 16a*. This corresponds to a 34% decrease in $\bar{\lambda}$ in the crystalline region relative to the amorphous matrix. ($\bar{\lambda}_m = 6.1$, $\bar{\lambda}_c = 4.0$).

Type 2b interactions involve craze propagation through lamellae which are principally flat-on. Volume fractions in the matrix range from 0.20 to 0.25 ($\bar{\lambda} = 4.4$). Where the craze intersects the spherulite, the thickness and volume fraction increase and decrease, respectively. This is the exact opposite of type 2a behaviour.

For the example shown in *Figure 16b*, the width of the craze increases approximately 15%. The fibril extension ratio increases from $\bar{\lambda}_m = 4.4$ in the matrix to $\bar{\lambda}_c = 4.8$ in the spherulite. This indicates that the craze can thicken more easily when encountering flat-on lamellae than when intersecting edge-on lamellae.

Case 3. There are four general types of behaviour in case 3; these interactions are characterized by the craze path proceeding directly through the centre of the spherulite, and are shown in *Figures 17–20*. The most striking feature is the disruption of the fibril structure in the craze at the centre of the spherulite. In uniaxial tension, fibril growth occurs parallel to the direction of the applied tensile stress. Type 3 interactions appear to have fibril 'bundles' in the craze near the central core of the spherulite.

The first two types are analogous to type 2, but the craze passes through the spherulite on a diameter instead of passing through peripheral lamellae. In case 3a (*Figure 17*), the craze propagates directly through the centre of the spherulite with only small deviations from its original path. The craze moves primarily through edge-on lamellae and curves to follow the splayed lamellae of the sheaf structure. Comparison of *Figures 17* and *16b* shows that the geometry is very similar, with the craze propagating along the axis of the spherulite sheaf, but the results are very different. The craze thickness remains relatively constant even inside the spherulite, and a large amount of non-fibrillar material is visible in the craze through this region. These bundles of material show no particular orientation relative to the craze surface and yield very high values for V_f, ranging from 0.35 to 0.67. The large range in V_f values also yields a large range of fibril extension ratios, from 1.5 to 2.9.

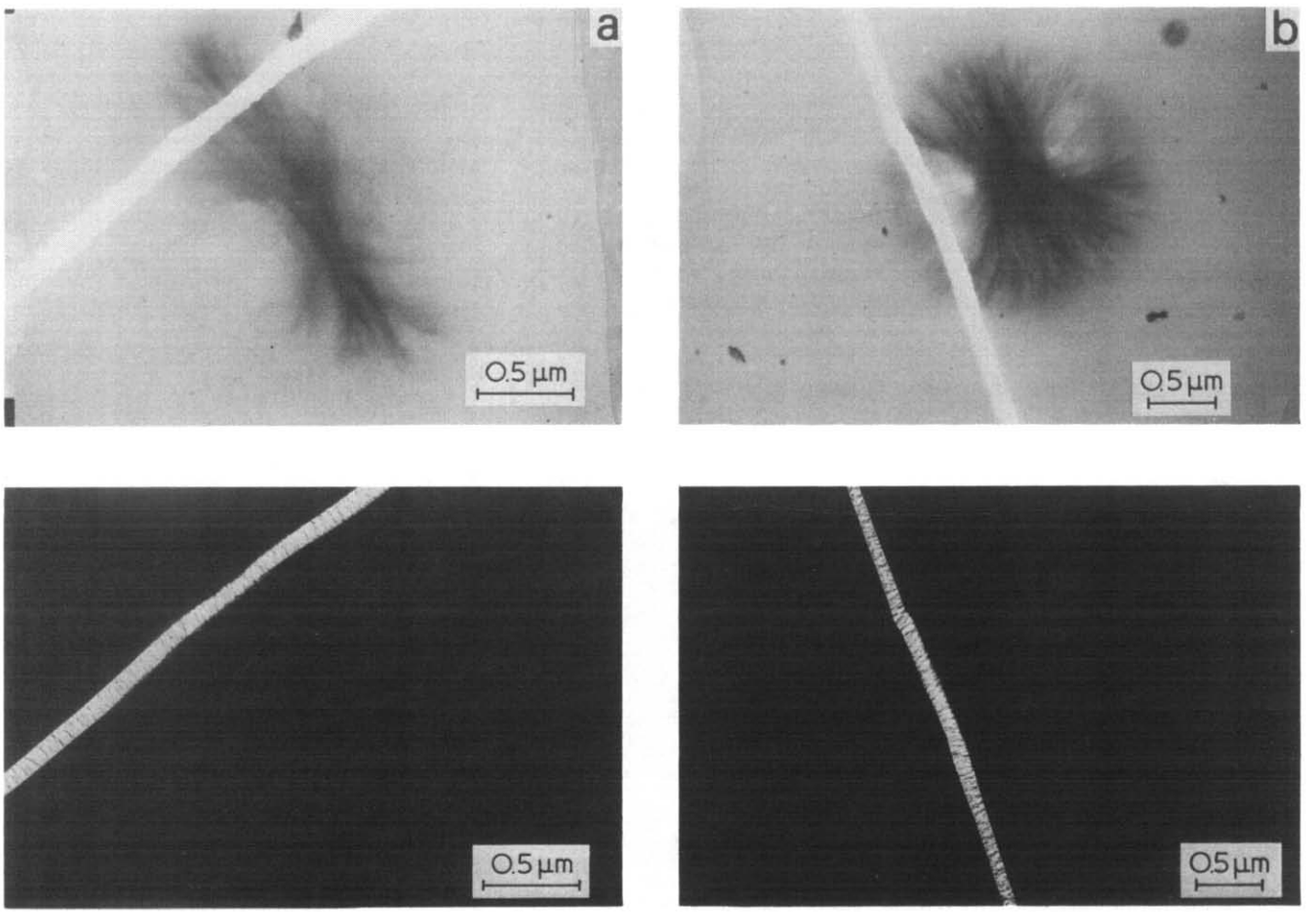

Figure 16 Electron micrographs showing type IIa (a) and type IIb (b) interactions where the craze passes through the periphery of the spherulite

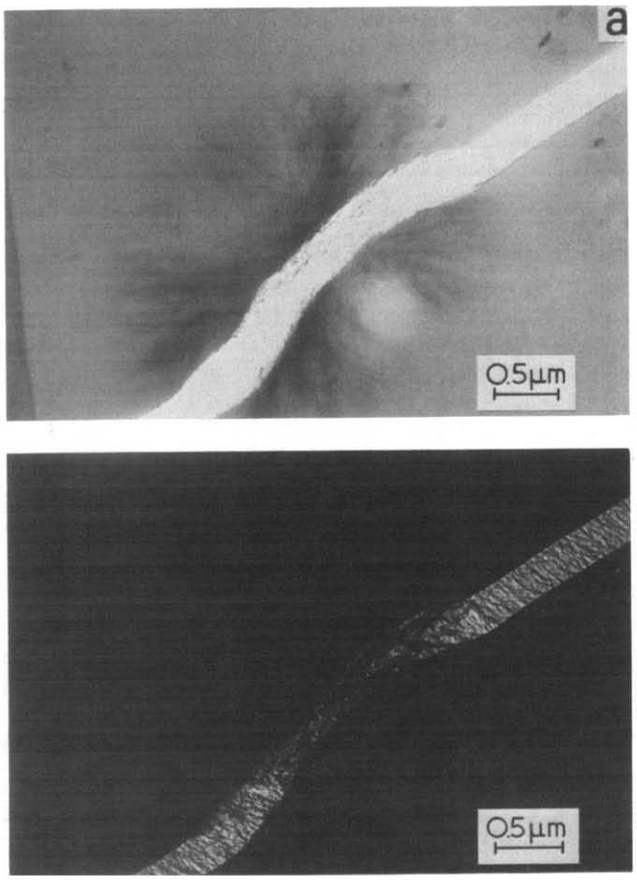

Figure 17 Electron micrographs of the first class of Type 3 interactions where the craze passes through the centre of the spherulite

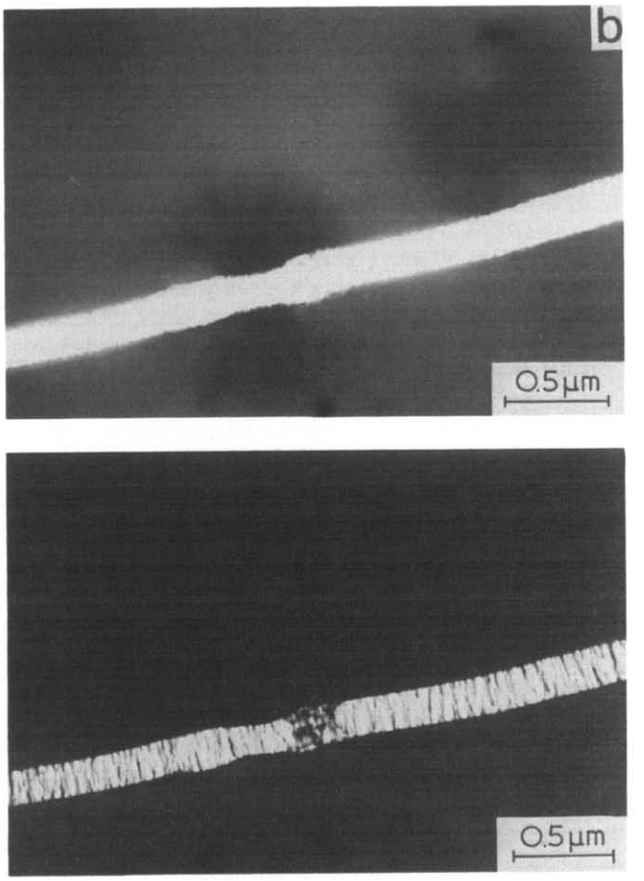

Figure 18 Electron micrographs of the second class of Type 3 interactions

In case 3b, *Figure 18*, the craze propagates directly through the spherulite centre *across* the sheaf axis, intersecting both flat-on and edge-on lamellae. (From the sheaf structure shown in *Figure 12*, it is impossible to pass through the spherulite centre without intersecting some edge-on lamellae.) Comparison of *Figure 18* and *16a* shows the similarity in overall geometry, but different lamellae are intersected, yielding different results.

The second two types of case 3 involve large deviations of the craze as it follows the radiating lamellae to the spherulite centre. These large deviations are most easily seen in larger, more developed spherulites. The deviations occur when the craze impinges on the spherulite on an off diametrical path, and intersects edge-on lamellae. If the craze meets edge-on lamellae on both sides of the spherulite centre, it will follow radial paths on both sides, resuming its original path when it re-enters the matrix (Type 3c, *Figure 19*).

In the regions of the spherulite where the craze intersects flat-on lamellae, the craze thickness increases slightly (0.20 to 0.26 μm) but the fibril volume fraction (and thus draw ratio) remain similar to the values in the matrix. V_f ranges from 0.18 to 0.24 with a $\bar{\lambda}$ of 4.8. Where the craze interacts with the spherulite centre (edge-on lamellae) the craze thickness decreases from 0.2 to 0.15 μm. V_f ranges from 0.26 to 0.62, yielding a $\bar{\lambda}$ of 2.3. This behaviour is similar to that observed in other type 3 interactions where the craze intersects edge-on lamellae. At the geometrical centre of the spherulite, the thickness of the craze has decreased to 30% of its initial value. The craze then proceeds out of the spherulite, following the edge-on lamellae, and exits on a path parallel to its initial direction. This is shown in the micrographs of *Figure 19*.

The fibril structure of the craze inside the spherulite is highly distorted. V_f is highest at the centre of the spherulite, where a draw ratio of approximately 1.4 was calculated ($V_f=0.71$). This was the lowest draw ratio observed, and indicates the difficulty the craze encounters in thickening at the spherulite core.

In Type 3d, the craze deviates to follow a radial path only on one side of the spherulite, and then continues on a path parallel to, but displaced from, its original path, *Figure 20*. It seems clear that on the right hand side the craze is passing through a flat-on region and on the left hand side through an edge-on region. However, on the left side, particularly towards the periphery of the spherulite, the volume fraction of the craze is very low, much more like that of a flat-on region. In both *Figures 19* and *20*, narrow sections of the two orientations are interspersed, and it is not always possible to be sure of the orientation of the lamellae which have been destroyed by the craze in these larger spherulites. Only the flat-on side of *Figure 12d*, which gives $V_f=0.18$–0.22, $\bar{\lambda}=5.0$, is used here.

Case 4. Craze tips are often observed embedded in spherulites, as shown in *Figure 21*. The structural and mechanical anisotropy associated with the spherulite result in the craze tip being highly distorted, and similar in appearance to tilted images of craze tips in a-PS where it has been shown that craze tips advance by a meniscus instability mechanism[6]. In a spherulite, the advancing

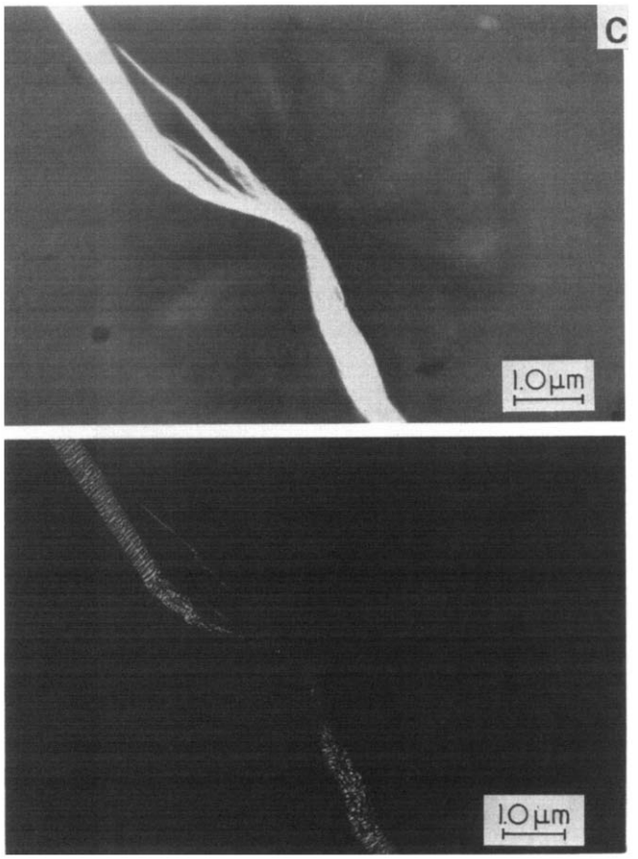

Figure 19 Electron micrographs of the third class of Type 3 interactions

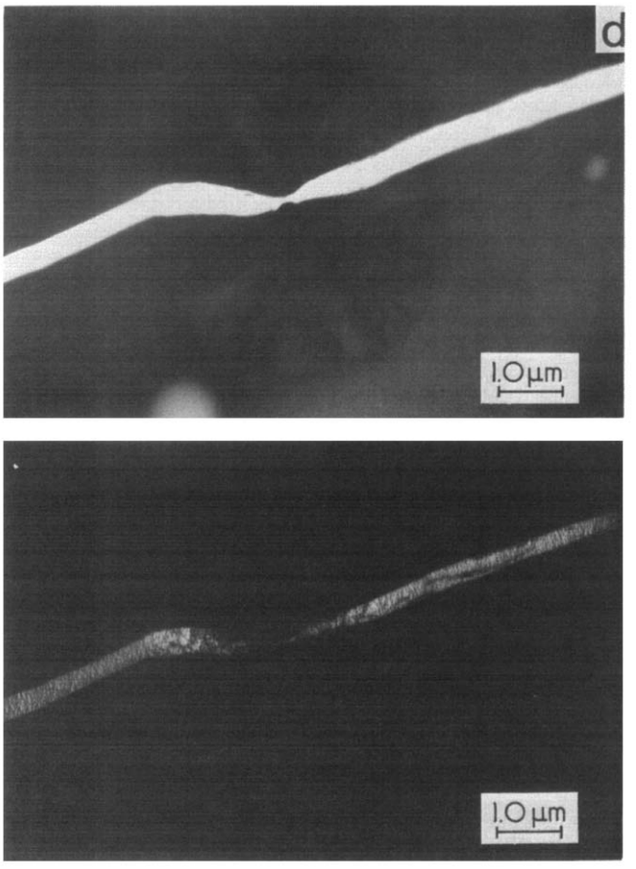

Figure 20 Electron micrographs of the fourth class of Type 3 interactions

'fingers' can move through either the interlamellar amorphous layers or the crystalline lamellae themselves. Because of the lower strength and stiffness of the amorphous material, the tip would be expected to advance more rapidly in these regions. This appears to occur in *Figure 21a*, where a thin line of lower mass thickness contrast is visible ahead of the craze tip, following the curvature of the lamellae in the sheaf.

For comparison, *Figure 22* shows a craze tip in amorphous i-PS; in this case, the tip is sharper and better defined. In the semi-crystalline films observed here, craze tips were observed in spherulites and in the amorphous matrix with a frequency approximately proportional to their relative area.

In all these cases, the V_f values shown in *Table 1* have been calculated from equation (1) using the optical density of the amorphous matrix near the spherulite for the value of ϕ_{film}. This assumption is clearly in error, for the micrographs in *Figures 16–20* show that the spherulite images have a different optical density than the amorphous matrix. The basis for equation (1) is that the volume of polymer remains constant during deformation, and ϕ_{film} is a measure of the mass thickness of the craze material before its deformation. Thus, although measurements of the optical density of spherulite regions adjacent to the crazes have been made, there is no guarantee that these values are the same as would have been obtained from the crazes prior to deformation.

Generally, the optical density of flat-on regions of spherulites in *Figures 16–20* is $\approx 10\%$ less than that of the surrounding amorphous material, and edge-on regions

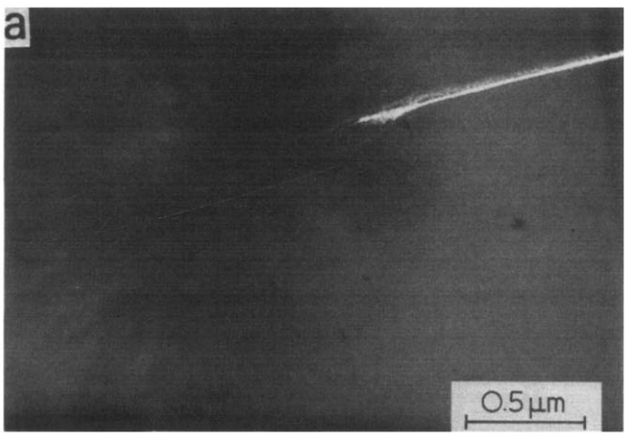

Figure 21 Electron micrograph of a Type IV interaction showing the craze tip inside the spherulite

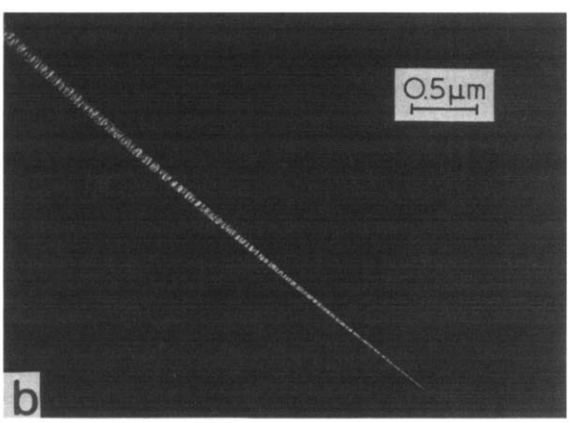

Figure 22 Electron micrograph of a craze tip in amorphous isotactic polystyrene

are ≈20% more dense, with considerable local variation. Applying the averaged correction to calculations of V_f and $\bar{\lambda}_s$ results in the corrected mean values at the bottom of *Table 1*. The true situation is even more complicated than this, for some of the difference in optical density between spherulite and matrix is due to radiation effects when the specimen is observed in the TEM[38]. These anisotropic distortions may or may not affect the calculated volume fractions and draw ratios, depending on the lamellar orientation and local mechanical constraints of the film. The correction is then less than the uncertainty in $\bar{\lambda}_s$ and $\bar{\lambda}_s/\bar{\lambda}_m$, and can be neglected. This is somewhat surprising, given the visibility of the spherulites in *Figures 16–20*, but the spherulite micrographs are taken at long exposure and processed to high contrast to make the spherulite visible, while the craze is intrinsically of very high contrast.

Interpretation of craze–spherulite interactions

The path and structure of crazes in spherulites are affected in many ways by the local elastic and plastic mechanical properties of the crystals and the composite properties of the spherulite. As these properties are not well known, crazes interacting with spherulites cannot be analysed in the detailed manner which was possible for crazes in the amorphous material. Even in the simplest case, Case 1, where only the elastic properties of the spherulite are involved and the craze remains in the amorphous matrix, an exact solution is not possible, and the magnitude of the stress concentration due to the spherulite can only be estimated by its effect on the craze draw ratio. The next simplest case is Case 4, where the tip stops in the spherulite. The local stress at the craze tip is less than the yield stress of the crystals at that point. As the deformation applied to the specimen is a strain step with stress relaxation, crazes also come to a half in the amorphous matrix. The fraction of tips which end in spherulites is approximately the area fraction of the film which is spherulitic; this implies that spherulites are not very effective craze stoppers, and the yield stress of the crystal composite is rarely higher than that of the amorphous material.

Deviations in the initial craze path to a radial path, as shown in *Figures 19* and *20*, can similarly be interpreted in terms of general yielding behaviour. Because the amorphous layers have a lower shear modulus and yield strength than the adjacent crystalline lamellae, the craze tip can deviate into the inter-lamellar regions with lower total energy than that required for a straight path. The craze tip follows the inter-lamellar path as long as it meets crystals which extend through the specimen film, e.g. 'edge-on'lamellae. Deviations from the initial path occur when the craze meets the crystals at an oblique angle, as from the corner of the film in *Figure 13*. This effect is seen most clearly in *Figure 19*. When the craze does not deviate, the most noticeable effect is the local change in volume fraction and draw ratio, and their dependence on crystal orientation.

Recently, a theory for craze micromechanics in glassy polymers has identified the entanglement network as the controlling feature of craze draw ratio[49]. The mean craze draw ratio is close to the limiting extension of the entanglement network for a wide range of polymers of different entanglement density[49]. If the mean contour length of chain between entanglements is l_e, the r.m.s. distance in the melt or the glass is:

$$d = (Kl_e)^{1/2} \tag{9}$$

where K is the Kuhn length of the material; the limiting extension ratio of a chain between two entangelements, λ_e, is given by:

$$\lambda_e = l_e/d = (l_e/K)^{1/2} \tag{10}$$

For PS, $l_e = 41$ nm[50], $K = 2.3$ nm, giving $d = 9.6$ nm and $\lambda_e = 4.3$. At an extension of λ_e, entanglements with mean separation d and an end-to-end vector parallel to the draw direction will be connected by taut chains. This is clearly too simple a model: the extensibility of a three-dimensional mathematical network will be greater than this by a factor of $3^{1/2}$, and chain fracture during drawing and void formation will also increase the extensibility[51]. However, a real network of self avoiding chains will not have the freedom or extensibility of a mathematical network. As the simple model has worked well for a-PS, it is also used in the following.

To apply the network concept to a semi-crystalline material, it is necessary to know the chain conformation in the lamellae. This is a topic on which there has been a great deal of interest and controversy[52]. In this case, crystallization occurred at 140°C, well below the temperature of peak growth rate (175°C) in a diffusion-controlled regime. Because i-PS does not crystallize to >50%, it is thus a case of large disorder, where the overall chain conformation should not be altered during crystallization. Experiments using small-angle neutron scattering (SANS) on exactly this system (i-PS of MW 10^5 crystallized at 140°C) have been published and show an unaltered molecular coil size[53]. Although the whole chain is unchanged, it is known that crystallization must effect the local conformation. The structure deduced from neutron scattering is that there are clusters of three closely spaced straight traverses of a single lamellar crystal, connected by long disordered chains in the interlamellar material[53]. From specimens stained in RuO_4 vapour[43], the lamellar thickness is 7 nm, and the interlamellar region is also 7 nm, giving a 50% crystallinity. Three traverses of a single lamellae require 21 nm of chain; for 50% crystallinity there must be 21 nm of chain in the amorphous interlamellar region, which conveniently yields a basic unit chain length approximately equal to l_e, the length between entanglements. This gives a very simple model for the mean conformation of a chain 41 nm long between two entanglement points. In the model, there are three crystal traverses by the chain, 7 nm along c, followed by a random coil of $21/2.3 = 9$ statistical units, with r.m.s. end-to-end distance 7 nm. Using the simple model described for the draw ratio, λ, yields:

$$\lambda_e \text{ parallel to } c = 410/(70+70) = 2.8$$

$$\lambda_e \text{ perpendicular to } c = 410/(70+10) = 5.0$$

When flat-on lamellae are drawn, it must always be perpendicular to c, and from *Table 1*, $\bar{\lambda}_s = 4.8 \pm 0.2$. However, edge-on crystals may be drawn either perpendicular to or parallel to the c-axis, as shown in *Figure 13*. In cases 3a and 3c, edge-on lamellae are drawn parallel to c, and in cases 2a and 3b, perpendicular to c. The draw ratio for case 2a is much greater than the other values in the edge-on group (*Table 1*); without it the mean draw ratio is 2.2. However, the matrix draw ratio with position in the craze (*Figures 4–8*) is best accounted for by considering the ratio $\bar{\lambda}_s/\bar{\lambda}_m$. The simple model described previously gives the ratios as:

$2.8/4.3 = 0.65$	Parallel to c
$5.0/4.3 = 1.2$	Perpendicular to c

From *Table 1*, the flat-on $\bar{\lambda}_s/\bar{\lambda}_m$ is 1.1 ± 0.2 and the edge-on 0.5 ± 0.1.

Attempts at providing a better model of chain conformation using statistical calculations of disordered chains in a lamellar structure[54] and enumerating the possible results of a distribution of cluster sizes produce results not very different from the simplest model. The results obtained in this manner are no more reliable because the calculated loops and tie molecules contain few statistical segments, and self avoidance will markedly affect the configurational statistics[54]. In any event, the calculated conformation would be symmetrical about the c-axis, and thus not explain the low $\bar{\lambda}_s$ of edge-on lamellae drawn perpendicular to c.

If the molecules form some sort of fold plane perpendicular to the growth direction, this would break the symmetry around the c-axis, but the effects of this should be most clearly seen in the 'flat-on' cases, where the lamellae may be deformed parallel to the growth direction (Case 2b) or perpendicular to it (3b), though perpendicular to c in both cases. The difference between these cases is not significant, indicating that there is no strongly preferred fold plane in this disordered system.

CONCLUSIONS

Air crazes in amorphous i-PS are similar, both structurally and mechanically, to those found in a-PS. The primary difference appears to be the greater fibril extension ratios obtained in i-PS near the craze tip. This leads to high fibril stresses in this region which may result in rapid fibril breakdown and crack growth. In fully spherulitic films of i-PS, the craze path is highly irregular, craze thickness varies widely from point to point, and the fibril structure is often disrupted. This is clearly illustrated when isolated craze–spherulite interactions are observed. It is found that the orientation of the lamellae relative to the craze path is significant in determining V_f (and thus λ) in those sections of the craze which lie inside the spherulite. Interactions with lamellae which are edge-on can cause large or small deviations in craze path, and visually cause a decrease in craze thickness with large local disruptions of the fibril structure. Inside the spherulite, this results in an increase in V_f (decrease in λ) relative to the amorphous matrix. When the craze propagates through regions of flat-on lamellae, the effects are not as pronounced as the edge-on case. No gross disruptions of fibril structure are seen, and locally only slight variations in craze thickness and V_f occur. Even in the two-dimensional case, a detailed analysis of local deformation behaviour is virtually impossible due to the mechanical anisotropy of the spherulites. However, a simple model based on local chain conformation in i-PS crystals correctly predicts the observed dependence of local draw ratio on crystal orientation. This behaviour should also occur in the three-dimensional case of deformation of complete spherulites.

ACKNOWLEDGEMENTS

Financial support and use of facilities through the Cornell Materials Science Center, which is funded by the National Science Foundation, is gratefully acknowledged. The authors would also like to thank Dr Robert Bubeck and Dow Chemical Company for supplying the isotactic polystyrene used in these experiments.

REFERENCES

1 Rabinowitz, S. and Beardmore, P. *Cri. Rev. Macromol. Sci.* 1972, **1**, 1
2 Kambour, R. P. *Macromol. Rev.* 1973, **7**, 1
3 Kramer, E. J. in 'Developments in Polymer Fracture' (Ed. E. H. Andrews), Chapman, 1979
4 Lauterwasser, B. D. and Kramer, E. J. *Phil. Mag.* 1979, **39**, 469
5 Donald, A. M., Chan, T. and Kramer, E. J. *J. Mat. Sci.* 1981, **16**, 669
6 Donald, A. M. and Kramer, E. J. *Phil. Mag.* 1981, **A43**, 857
7 Chan, T., Donald, A. M. and Kramer, E. J. *J. Mat. Sci.* 1981, **16**, 676
8 Beahan, P., Bevis, M. and Hull, D. *Phil. Mag.* 1971, **24**, 1267
9 Beahan, P., Bevis, M. and Hull, D. *Proc. Roy. Soc. Lond.* 1975, **A343**, 525
10 Beahan, P., Bevis, M. and Hull, D. *J. Mat. Sci.* 1972, **8**, 162
11 Hull, D. *J. Mat. Sci.* 1970, **5**, 357
12 Murray, J. and Hull, D. *Polymer* 1970, **10**, 451
13 Argon, A. S. and Hannosh, J. G. *Phil. Mag.* 1977, **A36**, 1195
14 Hull, D. in 'Polymeric Materials' (Ed. E. Baer and S. Y. Radcliffe), ASM, 1975
15 Keith, H. D. and Padden, F. J. *J. Appl. Phys.* 1964, **35**, 1270
16 Keith, H. D. and Padden, F. J. *J. Appl. Phys.* 1964, **35**, 1286
17 Bowden, P. B. and Young, R. J. *J. Mat. Sci.* 1974, **9**, 2034
18 Peterlin, A. *J. Mat. Sci.* 1971, **6**, 490
19 Peterlin, A. in 'Polymeric Materials' (Ed. E. Baer and S. Y. Radcliffe), ASM, 1975
20 Peterlin, A. *Polym. Eng. Sci.* 1977, **17**, 183
21 Keith, H. D. and Padden, F. J. *J. Polym. Sci.* 1959, **41**, 525
22 Yu, Y. F. and Ullman, R. *J. Polym. Sci.* 1962, **60**, 55
23 Cooney, J. L. *J. Appl. Polym. Sci.* 1964, **8**, 1889
24 Erhardt, P., Sasaguri, K. and Stein, R. S. *J. Polym. Sci.* 1964, **65**, 179
25 Ingram, P. and Peterlin, A. *J. Polym. Sci.* 1964, **B2**, 739
26 Sasaguri, K., Hoshino, S. and Stein, R. S. *J. Appl. Phys.* 1964, **35**, 47
27 Hay, J. L. and Keller, A. *Kolloid-Z* 1965, **204**, 43
28 Haas, T. W. and MacRae, P. H. *SPE J.* 1968, **24**, 28
29 Haas, T. W. and MacRae, P. H. *Polym. Eng. Sci.* 1969, **9**, 423
30 Allan, P. and Bevis, M. *Phil. Mag.* 1977, **35**, 405
31 Tarin, P. M. and Thomas, E. L. *Polym. Eng. Sci.* 1978, **9**, 423
32 Weynant, E., Haudin, J. M. and Sell, C. *J. Mat. Sci.* 1980, **15**, 2677
33 Donald, A. M. and Kramer, E. J. *J. Polym. Sci., Polym. Phys. Edn.* 1982, **20**, 899
34 Farrar, N. and Kramer, E. J. *Polymer* 1981, **22**, 691
35 Boon, J., Challa, G. and VanKrevelin, D. W. *J. Polym. Sci.* 1968, **A2,6**, 1791
36 Suzuki, T. and Kovacs, A. J. *Polymer J.* 1970, **1**, 82
37 Edwards, B. C. and Phillips, P. J. *Polymer* 1974, **15**, 351
38 Grubb, D. T. and Keller, A. *J. Mat. Sci.* 1972, **7**(131), 822
39 Grubb, D. T. *J. Mat. Sci.* 1974, **9**, 1715
40 Dlugosz, D. and Keller, A. *J. Appl. Phys.* 1968, **39**, 5776
41 Dlugosz, D., Grubb, D. T., Keller, A. and Rhodes, M. B. *J. Mat. Sci.* 1972, **7**, 142
42 Sneddon, I. N. 'Fourier Transforms', McGraw-Hill, NY, 1951, pp. 395–430
43 Morel, D. E. and Grubb, D. T. to be published
44 Donald, A. M. and Kramer, E. J. *Phil. Mag. A* 1981, **43**, 857
45 Bassett, D. C. 'Principles of Polymer Morphology', Cambridge University Press, Cambridge, Eng., 1981
46 Andrews, E. H. *Proc. Roy. Soc.* 1962, **A270**, 232
47 Andrews, E. H. *Proc. Roy. Soc.* 1964, **A277**, 562
48 Andrews, E. H. and Reeve, B. *J. Mat. Sci.* 1971, **6**, 547
49 Donald, A. M. and Kramer, E. J. *J. Polym. Sci., Polym. Phys. Edn.* 1982, **20**, 1129
50 Seitz, J. T. Presented at the 50th Golden Jubilee of the Rheological Society, Boston, 1979
51 Kramer, E. J. in (Adv. Polym. Sci.' (Ed. H. H. Kausch), **50**, Chap. 1 to be published
52 Grubb, D. T. *Faraday Soc. Disc.* 1979, **68**
53 Guenet, J-M. *Polymer*, 1981, **22**, 313
54 Guttman, C. M., D. Marzio, E. A. and Hoffman, J. D. *Polymer* 1981, **22**, 1466